Flow-Rate Estimation From Wellhead-Pressure and -Temperature Data

B. Izgec, SPE, Chevron Energy Technology Company; **A.R. Hasan,** SPE, University of Minnesota-Duluth; **D. Lin,** North Dakota State University; **C.S. Kabir,** SPE, Chevron Energy Technology Company*

Summary

Flow-rate metering has a less-than-satisfactory track record in the industry. Modern sensors offer a solution to this vexing problem. This paper offers two methods for estimating flow rates, predominantly from temperature data to complement-rate measurements. One approach consists of modeling the entire wellbore and requires both wellhead pressure (WHP) and wellhead temperature (WHT), whereas the other uses transient temperature formulation at a single point in the wellbore to compute the total production rate.

In the entire-wellbore approach, we use a wellbore model handling steady flow of fluids but unsteady-state heat transfer to estimate production rate, given wellhead pressure and temperature. The model rigorously accounts various thermal properties of the fluid and the formation, including Joule-Thompson (J-T) (Thompson and Joule 1853) heating and/or cooling. In the single-point approach, a single-point-temperature measurement made anywhere in the wellbore, including at the wellhead, is needed to estimate the mass rate at a given timestep. The method entails full transient treatment of the coupled fluid- and heat-flow problem at hand.

Examples from both gas and oil wells are shown to illustrate the application of the proposed methodology. Good correspondence between the measured and calculated results demonstrates the robustness of the proposed methods. These methods provide important rate information in various settings. For instance, in mature assets they can fill in the information void between tests or replace suspect rate data. Even well-instrumented wells can benefit because the methods can act as a verification tool, particularly in assets where integrated asset models are used to fine tune rate allocation. In addition, the single-point approach can provide the much needed rate information during pressure-transient tests.

Introduction

Individual well rates enter into a variety of engineering calculations. Paradoxically, the industry has struggled to meter this entity with decent accuracy. In fact, accuracy in flow metering has not kept pace with pressure and temperature measurements. Ordinarily, allocation algorithms are used to assign individual well rates from total production, unless a well is instrumented with a flowmeter. The lack of rigor of these allocation routines poses significant challenges during history matching of reservoir performance, particularly that involving rapidly changing events, such as coning or cresting of gas or water. In this context, test separators do not necessarily alleviate the metering issue simply because of inadequate flow time for large distances between a well and the point of separation, coupled with low test frequency. To compound the matter further, the industry has lacked motivations for accurate metering of nonessential entities, such as water, and to a large extent gas because of its flaring in many field operations. In a case study, Kabir and Young (2004) discussed some of the issues related to gas and water metering in a typical brownfield operation.

To enhance the quality of rate measurements at the individual wells, dedicated metering has evolved over the past two decades. However, direct metering of multiphase-fluid flow in a pipe is a difficult proposition because both volume fractions and the individual-phase velocities must be ascertained. Accordingly, flowmeters have been developed to handle complete, partial, and no separation of phases. Because gas-volume fraction increases with decreasing pressure, downhole metering at higher pressures can largely mitigate handling of the gas phase. Venturi-type flowmeters, requiring no separation of phases, have gained wide acceptance both downhole (Webster et al. 2006; Tibold et al. 2000; Brodie et al. 1995) and at the surface (Warren et al. 2001, Warren et al. 2003; Retnanto et al. 2001; Pinguet et al. 2006). Venturi-type flowmeter appears to have performed well in a comparative study reported by Busaidi and Bhaskaran (2003). Similar to Venturi, downhole fiber-optic flowmeters are another nonintrusive device that has undergone considerable field testing (Kragas et al. 2002, Kragas et al. 2003). Gas/liquid cylindrical cyclone (GLCC) technology (Kouba et al. 2006) separates gas from the liquid phases to facilitate ease of measurement at the surface. The liquids are metered on the basis of mass using the Coriolis principle (Liu et al. 1988). Oglesby et al. (2006) reported their field experiences with GLCCs while testing high-water-cut wells.

More recently, the increasing use of distributed temperature sensing (DTS) has led to profiling flow across different producing intervals (Ouyang and Belanger 2006, Johnson et al. 2006, Wang et al. 2008). The knowledge of the independent total rate at the wellhead allows appropriate zonal allocation of rate in accord with flow fraction. However, to our knowledge, estimation of total rate has not been demonstrated with temperature measurements alone. The intent of this work is to present two methods for estimating rates from temperature data independent of flow sensing. The intrinsic idea is to provide engineering tools to check on measurement quality and fill in the information void where infrequent measurements are being made, such as in a brownfield environment.

Theoretical Development

We describe two methods for estimating rate. The first method involves the entire wellbore in that both pressure-drop and the attendant heat-transfer calculations are performed. Note that the temperature difference is the prime driver for rate computation, and pressure-drop calculations play a secondary role. Here, the fluid flow occurs at steady state, while unsteady-state heat flow occurs in the formation. This method is, therefore, designated as the entire-wellbore approach. In the second method, we work with a single point in the wellbore by conserving mass, momentum, and energy in unsteady-state mode. This point may reside at any location in the wellbore where measurements occur, such as the wellhead. We term this approach the single-point method.

1. Entire-Wellbore Method. Our approach to estimating flow rate depends on the functional relationship between the production rate and the flowing-fluid temperature. Temperature difference between the wellbore fluid and its surrounding results in energy exchange. **Fig. 1** shows a typical offshore well with a number of changes in deviation angles and the temperature gradients for the surrounding.

As the hot reservoir fluid moves up the wellbore, it loses energy to the surrounding formation. This heat loss and the consequent fluid temperature depend on the mass-flow rate and thermal properties. For the usual case of a wellbore surrounded by earth, as shown in Appendix A, the mass-flow rate w is given by

* Now with Hess Corporation

This paper (SPE 115790) was accepted for presentation at the SPE Annual Technical Conference and Exhibition, Denver, 21–24 September 2008, and revised for publication. Original manuscript received for review 07 July 2008. Revised manuscript received for review 13 April 2009. Paper peer approved 18 April 2009.

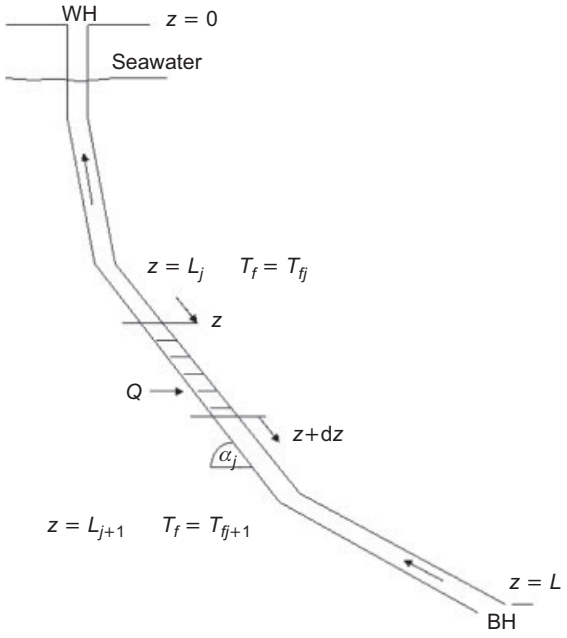

Fig. 1—Wellbore schematic for energy balance.

$$w \equiv \frac{2\pi r_{to} U_{to}}{c_p}\left[\frac{k_e}{k_e + \left(r_{to} U_{to} T_D\right)}\right]\frac{1}{L_R} = \frac{2\pi r_{to} U_{to}}{c_p}\left[\frac{k_e}{k_e + \left(r_{to} U_{to} T_D\right)}\right] f(T) \quad \ldots\ldots\ldots\ldots\ldots\ldots (1)$$

For the submerged section of an offshore well, the mass rate is written as

$$w = \frac{2\pi r_{to} U_{to}}{c_P} f(T). \quad \ldots\ldots\ldots\ldots\ldots\ldots\ldots\ldots\ldots\ldots (2)$$

In both Eqs. 1 and 2, the temperature function, $f(T)$, is given by

$$f(T) = \frac{\left(T_f - T_{ei}\right) - e^{(z-z_j)L_R}\left(T_{f_j} - T_{ei\,j}\right)}{\left(1 - e^{(z-z_j)L_R}\right)\left(g_G \sin\alpha + \phi - \frac{g\sin\alpha}{c_p}\right)}, \quad \ldots\ldots\ldots\ldots (3)$$

where ϕ lumps kinetic energy with the J-T coefficient, and is given by

$$\phi = \frac{v}{c_p J g_c}\frac{\mathrm{d}v}{\mathrm{d}z} - C_J \frac{\mathrm{d}p}{\mathrm{d}z}. \quad \ldots\ldots\ldots\ldots\ldots\ldots\ldots\ldots (4)$$

An iterative solution is required because both Eqs. 1 and 2 are implicit in w because f(T) contains L_R, which, in turn, requires knowledge of w for evaluation. Details of the solution algorithm appear in Appendix A.

2. Single-Point Method. Initiation of fluid production through the tubing creates temperature perturbation at any spatial point in the wellbore during each timestep. At a given point, amounts of energy brought from the reservoir and lost to the surroundings determine the changes in fluid temperature as a function of time. Under any production- and/or well-configuration scenario, the total production rate is the major contributor for the changes in temperature. We used a methodology that minimizes the difference between measured and model-calculated temperature by continuously iterating on the mass-flow rate. The Newton-Raphson method for mass-flux calculation at a single point is defined as

$$w_{l+1}^{k} = w_{l+1}^{k-1} - \frac{R_{l+1}^{k-1}}{\left(\partial R_{l+1}^{k-1} / \partial w_{l+1}^{k-1}\right)}, \quad \ldots\ldots\ldots\ldots\ldots\ldots (5)$$

where w is the total production rate in lbm/hr. The subscript $l + 1$ stands for new time level, and k represents the iteration number. The algorithm calculates the mass flow rate and uses it to generate temperature profiles through a temperature model. R is defined as a residual function and is given by

$$R = T_{fc} - T_{fm}. \quad \ldots\ldots\ldots\ldots\ldots\ldots\ldots\ldots\ldots\ldots (6)$$

The residual function is the temperature difference between the computed value, T_{fc}, and measured data, T_{fm}. Iteration continues until a satisfactory match is obtained between the two temperature values or the residual function is very close to zero. We used the following analytic temperature model (Hasan et al. 2005, Izgec et al. 2007a):

$$T_f = T_{ei} + \frac{1 - e^{-aL_R t}}{L_R}\left[1 - e^{(z-L)L_R}\right]\psi. \quad \ldots\ldots\ldots\ldots\ldots (7)$$

As detailed in Appendix A, the final form of the analytic derivative of the temperature model with respect to mass flux is given by

$$\frac{\partial T_{fc}}{\partial w_{l+1}} = \frac{1 - e^{-aL_R t}}{L_R'}\left[1 - e^{(z-L)L_R}\right]\psi, \quad \ldots\ldots\ldots\ldots\ldots (8)$$

and

$$L_R' = wL_R. \quad \ldots\ldots\ldots\ldots\ldots\ldots\ldots\ldots\ldots\ldots (9)$$

The analytic derivative of the residual function is

$$\frac{\partial R_{l+1}^{k-1}}{\partial w_{l+1}} = \frac{1 - e^{-aL_R t}}{L_R'}\left[1 - e^{(z-L)L_R}\right]\psi. \quad \ldots\ldots\ldots\ldots\ldots (10)$$

Note that this analytic derivative is imprecise because of the complicated nature of the temperature model. In particular, the exponential terms include mass-flux rate at the current timestep. But the iterative nature of the solution compensates for the lack of a complete differentiation with respect to mass-flux rate. However, the numeric derivative may be used to accelerate the convergence.

Calculation is initiated by assuming a mass rate at a given timestep, and then the fluid temperature is estimated with Eq. 7. Knowing the measured fluid temperature, T_{fm}, and computed fluid temperature, T_{fc}, the residual function is evaluated with Eq. 6. Thereafter, either the the analytic derivative (Eq. 10) or numeric (Eq. A-14) of the residual function is evaluated. Mass flux is then estimated with Eq. 5, followed by the fluid-temperature estimation with the new mass rate. This process is repeated until convergence is attained within a specified tolerance.

Example Applications

In this section, we present four examples. First, we generate a flow problem using a forward simulator (Izgec et al. 2007a) and analyze it with the unsteady-state approach to prove that the proposed methodology works in principle. Thereafter, three field examples show applications of both the entire-wellbore and single-point methods.

1. Synthetic Example for Proof of Concept. Consider production of single-phase oil from a 26,400-ft well. Temperature measurements are made at three locations **(Fig. 2),** corresponding to an imposed variable-rate history. Our objective is to reproduce the imposed rate profile, regardless of temperature measurements made at any point in the wellbore. Note that Fig. 2 also presents the computed temperature en route to computing the rate history. **Fig. 3** presents the rate match at 16,000 ft. As expected, the same-quality match is attained at other stations for the same flow problem at hand.

2. Multirate-Gas-Well Test Example. This example comes from a vertical gas well in a high-temperature reservoir, located in the US

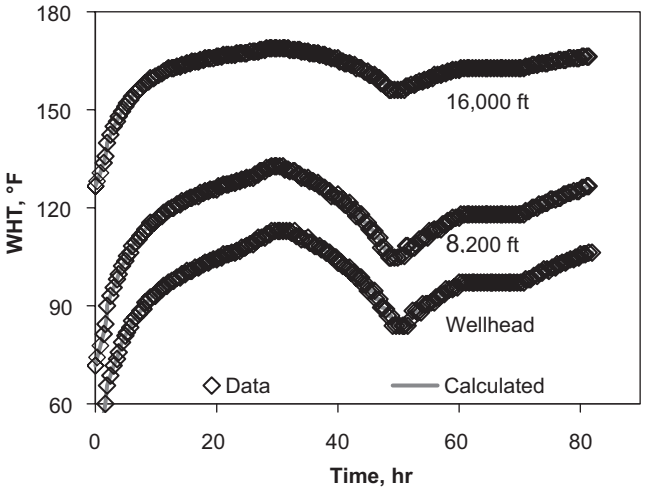

Fig. 2—Matching fluid temperature at various well depths.

Gulf Coast (Kabir et al. 1996). Pressure and temperature data were available both at bottomhole and wellhead from a multirate test. **Fig. 4** shows that the transient WHT was matched with the single-point method en route to computing rate. **Fig. 5** compares and contrasts the measured rates with those obtained from the two computational methods. One important difference between the entire-wellbore and single-point methods is that the transient nature of rate is captured by the latter. We think this is a significant development in that even many surface sensors may not be able to capture subtle rate variation during a transient test. Put another way, the ever-changing rate, which is a direct reflection of temperature, suggests dominating wellbore-storage effect in this 20,000-ft well with 0.35-md formation permeability.

Questions arise about the quality of the rate solution. We investigated the sensitivity of estimated flow rate with the entire-wellbore modeling approach. To illustrate the effect of temperature error on rate calculations, we considered the recorded WHT for the second rate period involving 10 MMscf/D. **Fig. 6** shows that the proposed method is quite robust. Indeed, rate estimation is not very sensitive to WHT; an error of 5°F in WHT leads to a 7% error in estimated rate.

3. Gas-Well Test With Wellbore Temperature Profile. This 7,000-ft dry gas well is vertical for the first 2,500 ft and deviates thereafter by 50° from vertical, terminating at a true vertical depth (TVD) of 5,412 ft. At a reported production rate of 50 MMscf/D, the WHT and bottomhole temperature (BHT) are 129°F and 150°F, respectively. A production log was also run, thereby providing us with a distributed-temperature profile throughout the wellbore. Because steady flow was prevalent for 48 hours, we invoked the entire-wellbore modeling approach. With three iterations, the

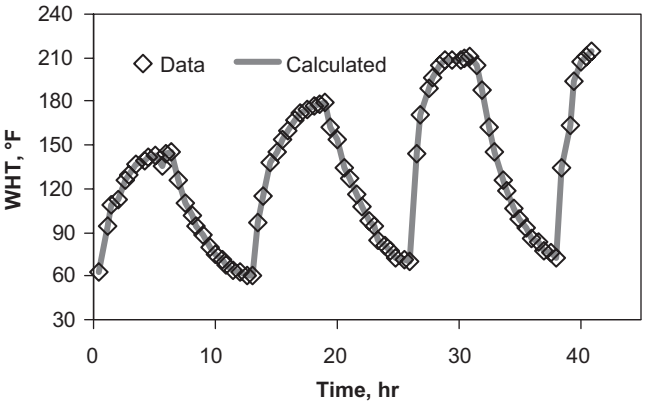

Fig. 4—Matching WHT with single-point approach.

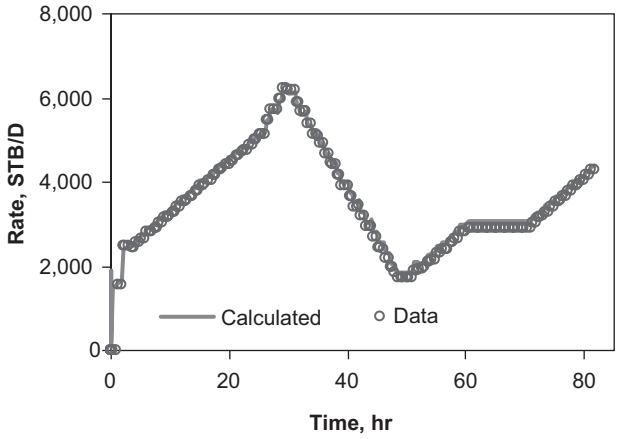

Fig. 3—Computed rate at 16,000 ft reproduces the input model rate profile.

model estimated a rate of 49.7 MMscf/D, which is in good agreement with the data. **Fig. 7** depicts the temperature-profile match obtained during history matching. While matching the temperature profile, we noted that approximating $(\partial Z/\partial T)_p$ by $(\Delta Z/\Delta T)$ along the well depth results in an inferior match. Note that the Z-factor derivative is required in Eq. A-9 en route to evaluating C_J in Eq. 4. When the Z-factor derivative is evaluated analytically, a much improved result is obtained. We used the Dranchuk and Abou-Kassem (1975) Z-factor formulation for this purpose.

We solved the same problem with the single-point approach. At each station, the same rate of 50 MMscf/D was calculated. However, we observed that the absolute error in the computed fluid temperature had an increasing trend with increasing depth. In particular, at the last station, the error is 1.63°F, as **Fig. 8** indicates. We think that this error is triggered by the diminished perturbation in measured temperature owing to significant decrease in heat transfer as the station approaches the producing interval. Nonetheless, if a permanent sensor is located too close to the producing interval, we can easily calibrate the model with a known rate measurement to allow accurate estimation at other flow conditions.

4. Tahiti Multirate-Oil-Well Test. This field example was discussed earlier by Izgec et al. (2007b). In this deepwater setting, a combined cleanup and shut-in period of approximately 70 hours preceded the variable-rate test, lasting approximately 60 hours. A shut-in test followed. Because of the transient nature of the flow problem, we invoked the single-point approach in estimating rate. **Fig. 9** depicts the temperature data measured at 9,600 ft measured depth (MD). The reservoir depth occurs at 26,500 ft MD. Also shown in Fig. 9 is the quality of temperature match, en route to computing the rate history. **Fig. 10** compares and contrasts the

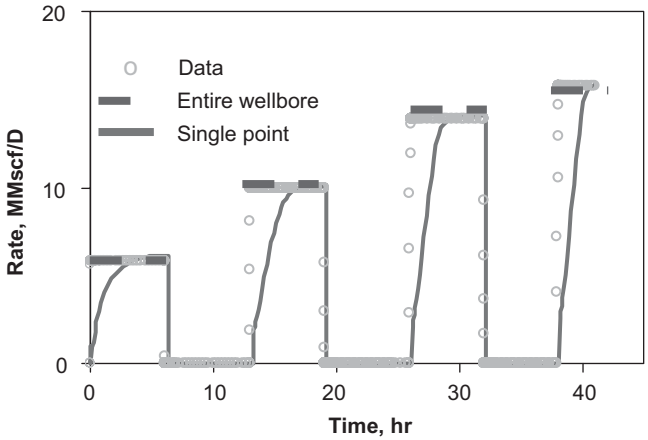

Fig. 5—Comparing measured and computed rates with both methods.

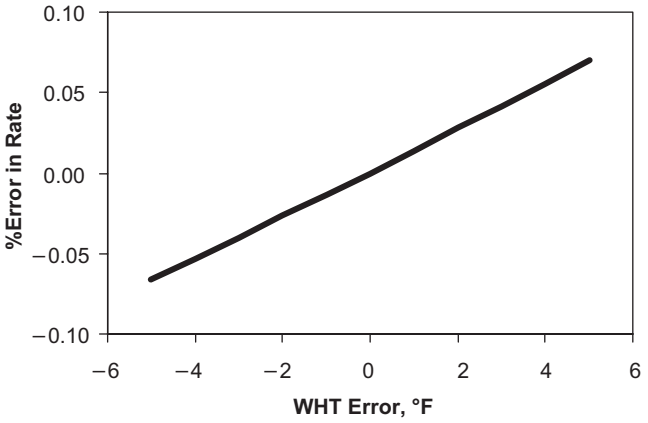

Fig. 6—How WHT error manifests in rate-calculation uncertainty.

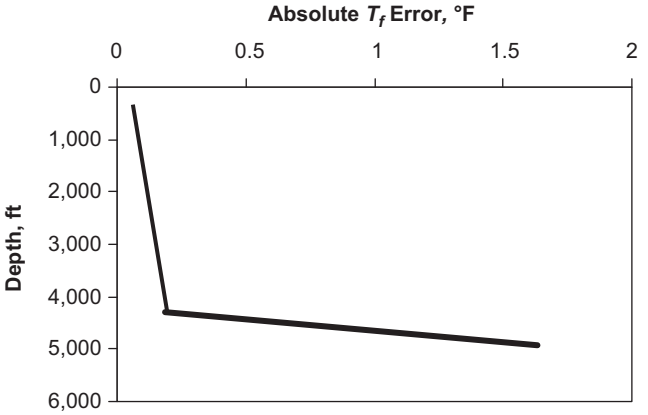

Fig. 8—Error in fluid-temperature estimation at each station with single-point approach.

computed-rate history with that measured at surface. Overall, the match appears good with the exception of those occurring at the highest rates. Physical limitations of rate-metering capability at the surface required that the rate in excess of 9,000 STB/D be diverted to another vessel. Issues with metering at the secondary facility precipitated the discrepancy in rate.

Let us explore how the computed-rate history impacts the pressure-buildup analysis that followed the 60-hour flow period, discussed earlier by Izgec et al. (2007b). The maximum discrepancy in rate is approximately 16%, occurring at approximately 25 hours.

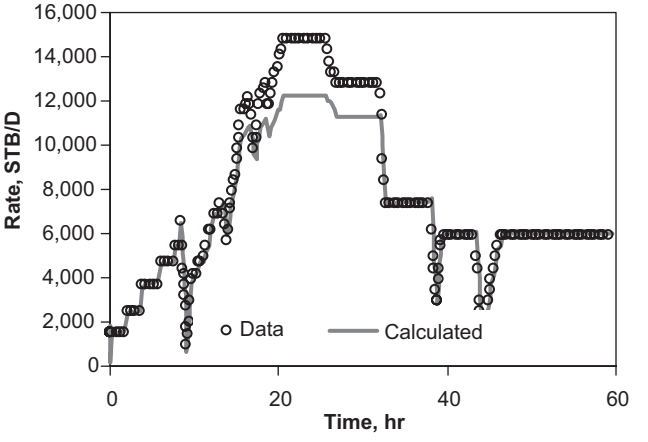

Fig. 10—Computed oil rate compares favorably with measured values.

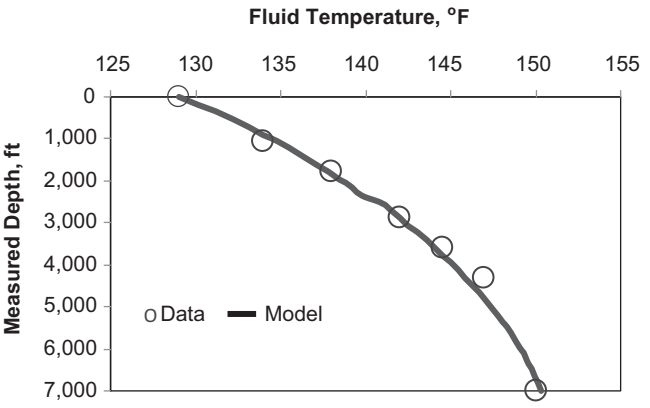

Fig. 7—Wellbore-temperature-profile match obtained en route to rate estimation with entire-wellbore approach.

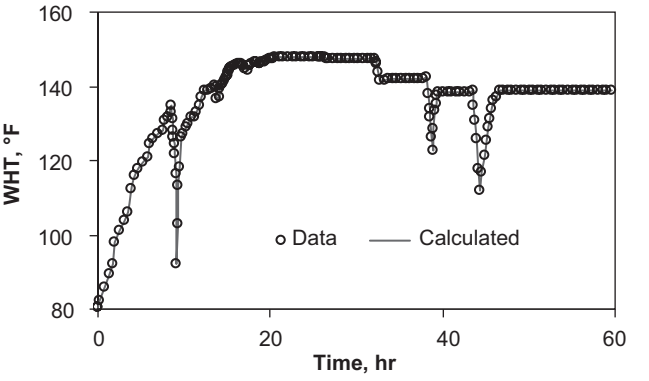

Fig. 9—Matching cell temperature at 9,600 ft MD.

Because the point of discrepancy occurs at a distant past relative to the buildup test, the error in the permeability-thickness product, *kh,* turns out to be minimal, only 2% lower than that estimated previously. However, had this rate discrepancy occurred just preceding the buildup test, the magnitude of error in *kh* estimation would have been directly proportional to the rate itself. This example underscores the importance of validating rate history before performing any transient analysis. Matching data at both ends of the peak rates provides confidence in our ability to compute rate from temperature measurements at any point in the wellbore.

5. Comparing and Contrasting Rate Solutions With Pressure and Temperature Models. In the entire-wellbore approach, we use both bottomhole and wellhead temperatures to estimate the rate. The accompanied pressure-traverse calculations simply allow accurate estimation of fluid properties, leading to superior energy balance. Intuitively, one can use just the pressure-drop calculations to estimate the rate, with simplifying assumptions for the heat-transfer component. To explore the feasibility of such an approach, let us compare and contrast solutions of both approaches.

Consider single-phase oil flow in a 4,525-ft vertical well producing 2,000 STB/D of 15°API oil. **Fig. 11** shows sensitivity of the estimated rate to errors in temperature and pressure modeling. Clearly, the rate-estimation error from a pressure model is far greater than that from the temperature model for the same percentage error in modeling. The basis for our analysis is that the uncertainty in pressure and temperature models' estimation is usually of the same order, ± 2%.

The reason a pressure model performs poorly in oil wells is that change in pressure loss is primarily owing to friction. As **Fig. 12** shows, for a four-fold change in rate (= 4-fold change in velocity, meaning 4^2 or 16-fold change in frictional loss), the static head changes by 3.2 psi, whereas frictional pressure loss changes by 108

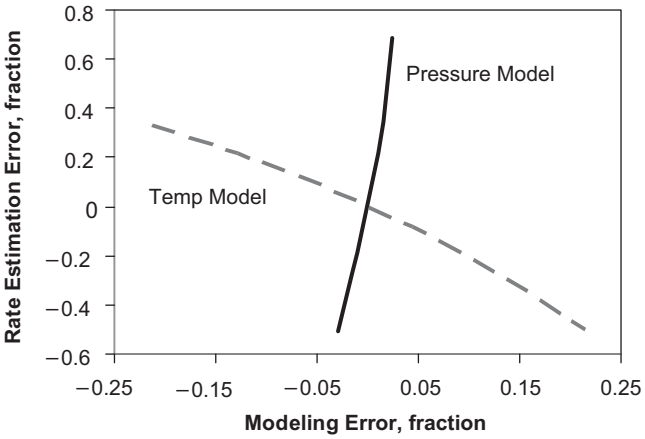

Fig. 11—Temperature model incurs much lower error than the pressure model.

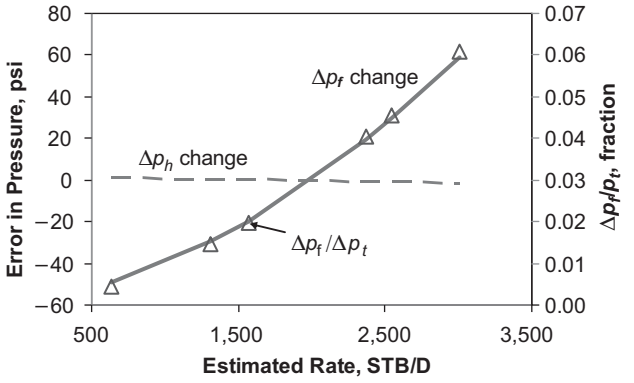

Fig. 12—Frictional-pressure-drop component dominates the total pressure drop.

psi. Therefore, to counteract the x psi error in pressure (either in data or in model estimation), the rate must change enough (proportional to square-root of x) for frictional loss to change by approximately x psi. However, friction is a very small fraction of the total pressure loss for vertical oil wells, as shown in Fig. 2. Thus, a 1.0% error in total Δp (= 0.01 × 1,913 psi for the base case = 19.1 psi) will require frictional pressure loss to change by approximately 16%. This 16% frictional pressure loss requires the rate to change by approximately 200 STB/D, thereby explaining the large percent error in rate estimation with the pressure model.

When a well produces water with oil, additional information/model must be available for estimating the two unknowns, production rate and water cut (WC). However, if the WC is known, the same thermal wellbore model allows calculation of the total production rate. **Fig. 13** shows simulated data from the same 4,525-ft vertical well producing 2,000 STB/D of 15°API oil at various WCs. Note that we assumed fluid homogeneity in the bubbly-flow regime (Hasan and Kabir 1999). The figure shows sensitivity of the estimated rate to temperature- (triangles) or pressure- (circles/squares) modeling error.

Water generally has higher density and specific heat than oil. Therefore, increased WC generally increases mixture density and enthalpy. Increased WC, in turn, causes higher Δp or decreased WHP and lower ΔT or increased WHT. However, as Fig. 13 shows, although the absolute errors in the estimated rate are different at various WCs, the trend remains the same for both the pressure and temperature models. Therefore, presence of water does not alter the picture, as far as the model's ability to handle water production is concerned.

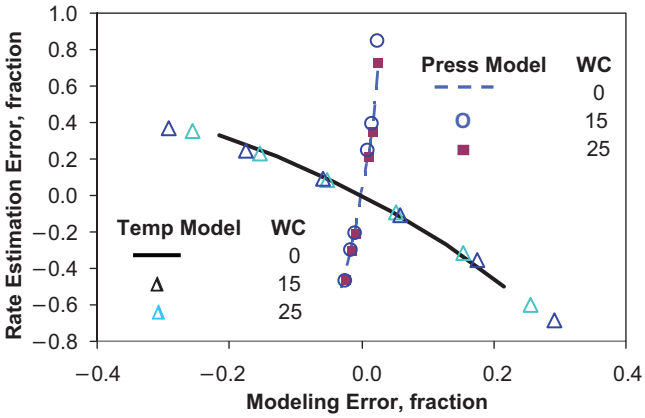

Fig. 13—Presence of water does not alter the error trend; superiority of the temperature model is demonstrated.

Note that if the produced oil is heavier, the changes in Δp will be smaller, causing difficulty in discerning any change in WC from changes in WHP. The same goes for temperature modeling—the closer the oil specific heat is to that of water, the more difficulty a temperature model will have in estimating WC. Put another way, independent measurement of WC is needed to estimate flow rate with the entire-wellbore model. In this context, let us point out that even multiphase-flow sensors need constant updating to accommodate ever-changing fluid pressure/volume/temperature (PVT) properties, albeit subtle, with reservoir depletion.

Discussion

In this study, we have verified both methods with example applications. The two methods offer relative strengths, however. In the entire-wellbore approach, the tubular and cement-sheath dimension and fluid, tubular, and formation thermal properties are needed as input parameters. Because the method relies upon modeling fluid and heat flows in the entire wellbore, both WHP and WHT are required. In this method, the entire wellbore is modeled in a bottom-up mode en route to seeking convergence with WHT and WHP, thereby instilling confidence in the solutions. By contrast, the single-point method is more flexible in that it requires only the temperature measurement at any point in the wellbore, plus the attendant fluid and thermal properties of the media at that point. Of course, the method needs the overall-heat-transfer coefficient at the point of temperature measurement and is evaluated with an iterative scheme, as discussed in Appendix A. Because this method relies on a point measurement, the approach offers the advantage of being applicable in a large variety of well completion and instrumentation.

In their current formulations, both methods presuppose that wellbore fluid and thermal storage effects are minimal. These conditions are well satisfied in single-phase flow in high-permeability-thickness (kh) reservoirs, particularly for the single-point method. The Tahiti example satisfies this condition rather well, and so does the synthetic example illustrating the method's ability to capture rate transients solely from temperature measurements. However, in a low-kh reservoir with a long compressible-fluid column, thermal transients may outlast fluid-storage effects, leading to a long period of time for the rate stabilization to occur. This point is illustrated by the Gulf Coast gas example where the low-kh formation and 20,000-ft wellbore trigger a rather long stabilization time. In contrast, the other gas example with distributed-temperature measurement exhibits rapid rate stabilization owing to the high-kh formation.

Potential applications of either method span a large spectrum of situations. For instance, rate allocation has a large uncertainty bar in most business settings. Either method can work well after calibration is attained with dedicated well measurements. Many well completions prevent placement of permanent sensors close to perforations. In this setting, the single-point method offers an

opportunity to capture rate because off-bottom measurements will allow significant heat transfer between the wellbore fluid and the formation, leading to significant temperature perturbation. While such off-bottom measurements pose a challenge in estimating formation parameters with pressure-transient analysis (Izgec et al. 2007b), they offer a better opportunity for estimating rate. Exploration-well testing is another area where the single-point method appears particularly appealing. The Tahiti test is a case in point. In all cases, we view the proposed methods to be complementary to conventional metering.

Conclusions

1. This study presents two independent methods for computing rate, predominantly from temperature measurements. In the entire-wellbore approach, both WHT and WHP are matched en route to estimating flow rate. In contrast, the single-point method works off of temperature measured at any point in the wellbore.
2. Field data corroborate the estimated rates for both gas and oil wells. Limited computational results suggest that the single-point method is capable of capturing transient rates, provided fluid and thermal storage effects are minimal at the point of interest.
3. The proposed methods provide a vital tool for checking rates even in well-instrumented systems, without any overhead.
4. Superiority of the temperature model over its pressure counterpart in the entire-wellbore approach is demonstrated.

Nomenclature

a = thermal parameter defined by Eq. 19, ft/hr
c_p = specific-heat capacity of fluid, Btu/lbm-°F
C_J = Joule-Thompson coefficient, (°F)/(lb_f/ft^2)
C_T = thermal storage parameter, dimensionless
g = gravitational acceleration, ft/sec^2
g_c = conversion factor, 32.17 lbm-ft/lbf/sec^2
g_G = geothermal gradient, °F/ft
h = formation thickness, ft
H = fluid enthalpy, Btu/lbm
J = Btu to ft-lbf conversion factor
k = formation permeability, md
k_a = thermal conductivity of annular fluid, Btu/hr-ft-°F
k_e = thermal conductivity of Earth, Btu/hr-ft-°F
L_R = relaxation parameter defined by Eq. A-2 or A-3, ft^{-1}
L = measured depth of wellbore, ft
L_j = measured (from wellhead) depth of section j of wellbore, ft
m = mass of fluid, lbm
M_g = molecular weight of the free gas, lbm/lb mole
p = pressure, psi
Δp_f = frictional pressure drop, psi
Δp_h = hydrostatic pressure drop, psi
Δp_t = total pressure drop, psi
q_o = oil-flow rate, STB/D
Q = heat-flow rate per unit length of wellbore, Btu/hr/ft
r_w = wellbore radius, ft
R = residual, defined by Eq. 13, °F
s = mechanical skin, dimensionless
t = producing time, hours
t_D = dimensionless time, hours
T_D = dimensionless temperature
T_e = earth or formation temperature, °F
T or T_f = fluid temperature, °F
T_{fc} = computed fluid temperature, °F
T_{fm} = measured fluid temperature, °F
T_{ei} = undisturbed-earth or -formation temperature, °F
T_{wb} = wellbore/earth-interface temperature, °F
U_{to} = overall-heat-transfer coefficient, Btu/hr-ft^2-°F
v = velocity, ft/s
V = fluid specific volume (=1/ ρ), ft^3/lbm
w = mass rate, lbm/hr
x = gas mass fraction (quality), dimentionless
z = variable well depth from surface, ft
Z = gas-compressibilty factor, dimensionless
α = well inclination (to horizontal) angle, degree
β = volume expansivity, $°F^{-1}$
γ_o = oil gravity, °API
γ_g = gas gravity (air = 1), dimensionless
μ = fluid viscosity, cp
ρ = fluid density, lbm/ft^3
ρ_e = Earth or formation density, lbm/ft^3
ϕ = lumped parameter defined by Eq. 9, °F/ft
σ = standard deviation of pressure, psi
$\psi = g_G \sin\theta + \phi - (g \sin\theta / c_p J g_c)$, °F/ft
θ = well deviation from vertical, degrees

Subscripts

c = calculated
e = earth (formation)
ei = initial earth contion (for temperature)
f = fluid
l = timestep
m = measured

Acknowledgment

We appreciate the input of many colleagues for providing the field data and thank Chevron management for permission to publish this work.

References

Ayala, L.F. 2006. On the non-ideality of hydrocarbon fluids: Implications for natural gas engineering–Part B. *E-Journal of Reservoir Engineering* **1** (1): 1–9.

Brodie, A.D., Allan, J.C., and Hill, G. 1995. Operating Experience With ESP's and Permanent Downhole Flowmeters in Wytch Farm Extended-Reach Wells. *JPT* **47** (10): 902–906. SPE-28528-PA. doi: 10.2118/28528-PA.

Busaidi, K. and Bhaskaran, H. 2003. Multiphase Flow Meters: Experience and Assessment in PDO. Paper SPE 84505 presented at the SPE Annual Technical Conference and Exhibition, Denver, 5–8 October. doi: 10.2118/84505-MS.

Dranchuk, P.M. and Abou-Kassem, J.H. 1975. Calculation of *Z*-factors for natural gases using equation of state. *J. Cdn. Pet. Tech.* **14** (3)**:** 34–36.

Hasan, A.R. and Kabir, C.S. 1999. A Simplified Model for Oil/Water Flow in Vertical and Deviated Wellbores. *SPE Prod & Fac* **14** (1): 56–62. SPE-54131-PA. doi: 10.2118/54131-PA.

Hasan, A.R., Kabir, C.S., and Lin, D. 2005. Analytic Wellbore-Temperature Model for Transient Gas-Well Testing. *SPE Res Eval & Eng* **8** (1): 240–247. SPE-84288-PA. doi: 10.2118/84288-PA.

Hasan, A.R., Kabir, C.S., and Wang, X. 2009. A Robust Steady-State Model for Flowing-Fluid Temperature in Complex Wells. *SPE Prod & Oper* **24** (2): 269–276. SPE-109765-PA. doi: 10.2118/109765-PA.

Izgec, B., Cribbs, M.E., Pace, S.V., Zhu, D., and Kabir, C.S. 2007b. Placement of Permanent Downhole Pressure Sensors in Reservoir Surveillance. *SPE Prod & Oper* **24** (1): 87–95. SPE-107268-PA. doi: 10.2118/107268-PA.

Izgec, B., Kabir, C.S., Zhu, D., and Hasan, A.R. 2007a. Transient Fluid and Heat Flow Modeling in Coupled Wellbore/Reservoir Systems. *SPE Res Eval & Eng* **10** (3): 294–301. SPE-102070-PA. doi: 10.2118/102070-PA.

Johnson, D., Sierra, J., and Gualtieri, D. 2006. Successful Flow Profiling of Gas Wells Using Distributed Temperature Sensing Data. Paper SPE 103097 presented at the SPE Annual Technical Conference, San Antonio, Texas, USA, 24–27 September. doi: 10.2118/103097-MS.

Kabir, C.S. and Young, N.J. 2004. Handling Production-Data Uncertainty in History Matching: The Meren Reservoir Case Study. *SPE Res Eval & Eng* **7** (2): 123–131. SPE-87823-PA. doi: 10.2118/87823-PA.

Kabir, C.S., Hasan, A.R., Jordan, D.L., and Wang, X. 1996. A Wellbore/Reservoir Simulator for Testing Gas Wells in High-Temperature Reservoirs. *SPE Form Eval* **11** (2): 128–134. SPE-28402-PA. doi: 10.2118/28402-PA.

Kouba, G., Wang, S., Gomez, L., Mohan, R., and Shoham, O. 2006. Review of the State-of-the-Art Gas/Liquid Cylindrical Cyclone (GLCC) Technology—Field Applications. Paper SPE 104256 presented at the International Oil & Gas Conference and Exhibition in China, Beijing, China, 5–7 December. doi: 10.2118/104256-MS.

Kragas, T.K., Johansen, E.S., Hassanali, H., and Da Costa, S.L. 2003. Installation and Data Analysis of a Downhole, Fiber Optic Flowmeter at Mahogany Field, Offshore Trinidad. Paper SPE 81018 presented at the SPE Latin American and Caribbean Petroleum Engineering Conference, Port-of-Spain, Trinidad and Tobago, 27–30 April. doi: 10.2118/81018-MS.

Kragas, T.K., van der Spek, A., and Al-Hashmi, K.M. 2002. Field Trial of a Downhole, Fiber Optic, Two-Phase Flowmeter in PDO's Nimr Field. Paper SPE 78306 presented at the European Petroleum Conference, Aberdeen, 29–31 October. doi: 10.2118/78306-MS.

Liu, K.T., Canfield, D.R., and Conley, J.T. 1988. Application of a Mass Flowmeter for Allocation Measurement of Crude Oil Production. *SPE Prod Eng* **3** (4): 633–636. SPE-15394-PA. doi: 10.2118/15394-PA.

Oglesby, K.D., Mehdizadeh, P., and Rodger, G.J. 2006. Portable Multiphase Production Tester for High-Water-Cut Wells. Paper SPE 103087 presented at the SPE Annual Technical Conference and Exhibition, San Antonio, Texas, USA, 24–27 September. doi: 10.2118/103087-MS.

Ouyang, L.-B. and Belanger, D. 2006. Flow Profiling by Distributed Temperature Sensor (DTS) System—Expectation and Reality. *SPE Prod & Oper* **21** (1): 269–281. SPE-90541-PA. doi: 10.2118/90541-PA.

Pinguet, B.G., Roux, G., and Hopman, N. 2006. Field Experience in Multiphase Gas-Well Testing: The Benefit of the Combination of Venturi and Gamma Ray Fraction Meter. Paper SPE 103223 presented at the SPE Annual Technical Conference and Exhibition, San Antonio, Texas, USA, 24–27 September. doi: 10.2118/103223-MS.

Ramey, H.J. 1962. Wellbore Heat Transmission. *J. Pet Tech* **14** (4): 427–435; *Trans.,* AIME, **225**. SPE-96-PA. doi: 10.2118/96-PA.

Retnanto, A., Weimer, B., Kontha, I.N.H., Triongko, H., Azim, A., and Kyaw, H.A. 2001. Production Optimization Using Multiphase Well Testing: A Case Study From East Kalimantan, Indonesia. Paper SPE 71556 presented at the SPE Annual Technical Conference and Exhibition, New Orleans, 30 September–3 October. doi: 10.2118/71556-MS.

Thompson, W. and Joule, J.P. 1853. On the Thermal Effects of Fluids in Motion. *Phil. Trans. R. Soc. Lond.* **143**: 357–365. doi:10.1098/rstl.1853.0014.

Tibold, M.P., Simonian, S., Chawla, M., and Akbar, M. 2000. Well Testing with a Permanent Monitoring System. Paper SPE 63079 presented at the SPE Annual Technical Conference and Exhibition, Dallas, 1–4 October. doi: 10.2118/63079-MS.

Wang, X., Lee, J., Thigpen, B., Vachon, G., Poland, S., and Norton, D. 2008. Modeling Flow Profile Using Distributed Temperature Sensor (DTS) System. Paper SPE 111790 presented at the Intelligent Energy Conference and Exhibition, Amsterdam, 25–27 January. doi: 10.2118/111790-MS.

Warren, P.B., Al-Dusari, K.H., and Al-Abduljabbar, J.M. 2003. Field-Testing a Compact Multiphase Flow Meter—Offshore Saudi Arabia. Paper SPE 81560 presented at the Middle East Oil Show, Bahrain, 9–12 June. doi: 10.2118/81560-MS.

Warren, P.B., Hussain, S., and Ghamdi, S. 2001. Background and Operational Experience of Multiphase Metering in the Safaniya Field—Offshore Saudi Arabia. Paper SPE 71534 presented at the SPE Annual Technical Conference and Exhibition, New Orleans, 30 September–3 October. doi: 10.2118/71534-MS.

Webster, M., Richardson, S., Gabard-Cuoq, C., Fitzgerald, J.B., and Stephenson, K.E. 2006. Well Surveillance With a Permanent Downhole Multiphase Flowmeter. *SPE Prod & Oper* **21** (3) 388–393. SPE-90024-PA. doi: 10.2118/90024-PA.

Appendix A: Rate-Estimation Models

Entire-Wellbore Method. Hasan et al. (2009) performed a general energy balance for the fluid, either single- or two-phase, to develop a first-order linear-differential equation describing the flow. With the boundary condition that fluid temperature at the measured distance, z_j (the "entrance" to the section), is known and is designated by T_{fj}, they developed the following analytic expression for fluid temperature:

$$T_f = T_{ei} + \frac{1-e^{(z-z_j)L_R}}{L_R}\left[g_G \sin\alpha + \varphi - \frac{g\sin\alpha}{c_p}\right] + e^{(z-z_j)L_R}\left(T_{f_j} - T_{eij}\right) \quad \ldots\ldots\ldots\ldots (A\text{-}1)$$

For a wellbore section surrounded by earth, the relaxation distance, L_R, is given by the following expression:

$$L_R \equiv \frac{2\pi}{c_p w}\left[\frac{r_{to}U_{to}k_e}{k_e + \left(r_{to}U_{to}T_D\right)}\right], \quad \ldots\ldots\ldots\ldots\ldots\ldots\ldots\ldots (A\text{-}2)$$

where the dimensionless temperature function, T_D, is calculated from dimensionless producing time, t_D, using the following expression:

$$T_D = \ln\left[e^{-0.2t_D} + \left(1.5 - 0.3719e^{-t_D}\right)\sqrt{t_D}\right]. \quad \ldots\ldots\ldots\ldots\ldots (A\text{-}3)$$

For a wellbore section submerged in water, L_R is given by

$$L_{Rc} = \frac{2\pi r_{to}U_{toc}}{c_p w}. \quad \ldots\ldots\ldots\ldots\ldots\ldots\ldots\ldots\ldots\ldots (A\text{-}4)$$

The dependence of fluid temperature on L_R and on mass rate, w, allows us to estimate the flow rate. Rewriting Eq. 1, we have

$$(T_f - T_{ei}) - e^{(z-z_j)L_R}(T_{f_j} - T_{eij}) = \frac{1-e^{(z-z_j)L_R}}{L_R}\left[g_G \sin\alpha + \varphi - \frac{g\sin\alpha}{c_p}\right]. \quad \ldots\ldots\ldots\ldots\ldots\ldots (A\text{-}5)$$

For the usual case of a wellbore surrounded by earth, as shown in Appendix A, the mass-flow rate w is given by rearranging Eq. A-2 as

$$w \equiv \frac{2\pi r_{to}U_{to}}{c_p}\left[\frac{k_e}{k_e + \left(r_{to}U_{to}T_D\right)}\right]\frac{1}{L_R} = \frac{2\pi r_{to}U_{to}}{c_p}\left[\frac{k_e}{k_e + \left(r_{to}U_{to}T_D\right)}\right]f(T). \quad \ldots\ldots\ldots\ldots\ldots\ldots (A\text{-}6)$$

For the submerged section of an offshore well when Eq. 4 applies, the term in the bracket in Eq. A-6 is replaced by 1, leading to

$$w = \frac{2\pi r_{to}U_{to}}{c_P} f(T). \quad \ldots\ldots\ldots\ldots\ldots\ldots\ldots\ldots\ldots\ldots (A\text{-}7)$$

In both Eqs. A-6 and A-7, the temperature function, $f(T)$, is given by

$$f(T) = \frac{\left(T_f - T_{ei}\right) - e^{(z-z_j)L_R}\left(T_{f_j} - T_{eij}\right)}{\left(1 - e^{(z-z_j)L_R}\right)\left(g_G \sin\alpha + \varphi - \frac{g\sin\alpha}{c_p}\right)}. \quad \ldots\ldots\ldots\ldots (A\text{-}8)$$

Expressions for Thermodynamic Parameters. The use of Eq. A-6 or A-7, along with Eq. A-8, requires an estimate of ϕ. Because ϕ is the sum of kinetic energy and J-T terms, a single empirical expression for it may lead to unacceptable errors. Many modern wells produce at very high rates, thereby making contribution of the kinetic energy term in ϕ significant. Large pressure gradients associated with high production rates also exacerbate the J-T effect. Additionally, not only is the J-T effect in low-pressure gas wells opposite to that of oil wells, the J-T effect in high-pressure gas wells is usually opposite to that in low-pressure gas wells (Ayala 2006, Hasan et al. 2009).

These thermodynamic considerations led us to evaluate the two terms in ϕ individually. Noting that for either single- or two-phase flow, $c_p C_J$ is given by $-[V-T(\partial V/\partial T)_p]$, Hasan et al. (2009) presented the following general expression for the J-T coefficient:

$$C_J c_p = \frac{xT}{ZM_g\rho_g}\left(\frac{\partial Z}{\partial T}\right)_p - (1-x)\frac{1-T\beta}{\rho_L}, \quad \ldots\ldots\ldots\ldots\ldots\ldots (A\text{-}9)$$

where Z is the gas compressibility factor ($\equiv VpM_g/RT$) and β is the liquid-volume expansivity, which is given by

$$\beta \equiv (1/V)(\partial V/\partial T)_p \equiv (-1/\rho)(\partial\rho/\partial T)_p. \quad \ldots\ldots\ldots\ldots\ldots\ldots (A\text{-}10)$$

Solution Algorithm. Examination of either Eq. A-6 or Eq. A-7 reveals that the expression is implicit in rate because $f(T)$ on the right side of Eq. A-6 contains L_R, which requires knowledge of w. Because w appears on both sides of the equations, an iterative solution approach is called for. We start with a trial value of L_R, use Eq. A-7 to estimate $f(T)$, estimate w from either Eq. A-6 or Eq. A-7, and recalculate L_R from Eq. A-2 or Eq. A-4. This process is repeated until two subsequent values of L_R are within a specified tolerance.

During steady-state production, the mass-flow rate passing through each point is the same. Nonetheless, properties such as geothermal gradient, number of casings, cement thickness, heat capacity, and thermal conductivity of the formation are different throughout the wellbore. For a simple well with a single deviation angle and geothermal gradient, the approach mentioned in the preceding can be used directly to calculate flow rate from wellhead data iteratively. However, as Hasan et al. (2009) pointed out, most wells traverse multiple geothermal gradients with varying deviation angles. Our heat-transfer modeling, therefore, discretizes the wellbore into a number of sections. Let us presuppose that bottomhole pressure (BHT), WHT, and WHP are known. However, neither the entire fluid temperature profile nor the BHP data are available. Computations start from the bottomhole assuming a rate and a BHP, leading to T_f estimation at a node above the bottom of the hole with Eq. A-1, and computation continues until the wellhead is reached. Differences in the calculated WHT and WHP with the measured data are used to estimate improved values of rate and BHP. The process is continued until an acceptable accuracy is attained.

Calculating an accurate pressure profile is as important as an accurate temperature profile because of their coupled nature. This fact becomes evident when one computes the J-T coefficient and ϕ value at each cell. For instance, a slightly erroneous value of C_J, which depends on pressure, will cause poor estimation of ϕ, leading to a significant error in the estimated temperature. An important lesson learned from these calculations is that a bottom-up computational approach is much superior to a top-down approach. Starting from the wellhead with an inaccurate set of data usually leads to increasing errors at each cell, with a strong tendency to diverge from the true solution. Calculations starting from the bottom of the well usually converge quickly.

Single-Point Method. The derivative of the residual function with respect to mass-flux rate at a given timestep is given as

$$\frac{\partial R_{l+1}^{k-1}}{\partial w_{l+1}} = \frac{\partial}{\partial w_{l+1}}\left[T_{fc} - T_{fm}\right]_{l+1}. \quad \ldots\ldots\ldots\ldots\ldots\ldots (A\text{-}11)$$

Expanding,

$$\frac{\partial R_{l+1}^{k-1}}{\partial w_{l+1}} = \frac{\partial T_{fc}}{\partial w_{l+1}} - \frac{\partial T_{fm}}{\partial w_{l+1}}. \quad \ldots\ldots\ldots\ldots\ldots\ldots (A\text{-}12)$$

The second term on the right-hand side drops out because field data are not affected by model-generated mass fluxes. The expression for the residual function then becomes

$$\frac{\partial R_{l+1}^{k-1}}{\partial w_{l+1}} = \frac{\partial T_{fc}}{\partial w_{l+1}}. \quad \ldots\ldots\ldots\ldots\ldots\ldots (A\text{-}13)$$

The derivative of model-calculated temperatures with respect to mass flux can be taken either numerically or analytically. The numeric expression can be shown as

$$\frac{\partial T_{fc}}{\partial w_{l+1}} = \frac{T_f^k - T_f^{k-1}}{w_{l+1}^k - w_{l+1}^{k-1}}. \quad \ldots\ldots\ldots\ldots\ldots\ldots (A\text{-}14)$$

The analytic derivative is dependent upon the temperature model employed. We used the following analytic temperature model (Hasan et al. 2005, Izgec et al. 2007a):

$$T_f = T_{ei} + \frac{1-e^{-aL_R t}}{L_R}\left[1-e^{(z-L)L_R}\right]\psi. \quad \ldots\ldots\ldots\ldots\ldots\ldots (A\text{-}15)$$

The derivative of temperature model with respect to mass-flux rate at the current timestep becomes

$$\frac{\partial T_{fc}}{\partial w_{l+1}} = \frac{\partial}{\partial w_{l+1}}\left[T_{ei} + \frac{1-e^{-aL_R t}}{L_R}\left[1-e^{(z-L)L_R}\right]\psi\right]. \quad \ldots\ldots\ldots (A\text{-}16)$$

In Eq. A-16, a is defined in terms of fluid mass in control volume per unit length ($m = \rho_f \pi r_t^2$) and the thermal-storage parameter C_T (Hasan et al. 2005) as

$$a = \frac{w}{m(1+C_T)}. \quad \ldots\ldots\ldots\ldots\ldots\ldots (A\text{-}17)$$

The thermal-storage parameter value depends on actual wellbore material and is usually 3 for drawdown and 2 for buildup. The term Ψ in Eq. A-17 lumps the geothermal gradient, ϕ, defined by Eq. 4, and the static head as

$$\psi = g_G \sin\theta + \varphi - \frac{g\sin\theta}{Jg_c c_p} \equiv g_G \sin\theta + \varphi - \frac{\sin\theta}{778.16 c_p}. \quad \ldots\ldots (A\text{-}18)$$

Appendix B: Estimating Upper and Lower Limits of the Overall-Heat-Transfer Coefficient

This section provides a simple diagnostic plot to estimate the range of the overall-heat-transfer coefficient (U_{to}) by graphing the model-generated-mass-flux rates with changes in fluid temperature relative to the initial condition at the point of interest. This method is illustrated by generating the mass-rate vs. temperature-difference plot for the Tahiti well example.

In this particular case, the data collection point was located approximately 1,000 ft below a salt feature with a complex completion scheme consisting of multiple sealed annuli and vacuum-insulated tubing to prevent annulus-pressure buildup. The resistances offered by multiple annuli and their trapped fluid, vacuum-insulated tubing, and the presence of a thick salt layer make theoretical estimation of the overall-heat-transfer coefficient difficult. **Fig. B-1,** which is generated with an U_{to} of 1.0 Btu/hr–ft^2–°F, suggests that the heat-transfer rate from the tubing fluid to the formation does not reach steady state even after 60 hours of production. This conclusion can be supported by a lack of any identifiable relationship between the mass flux and temperature difference.

Fig. B-2, on the other hand, displays a straight line at late times with U_{to} of 1.85 Btu/hr-ft^2-°F. This straight line signifies an established relationship between mass-flux rate and change in fluid temperature at the measurement depth. As shown earlier in Fig. 9, this U_{to} value provided the best match between the field-reported and model-generated rates. In this case, the early-time scatter disappears after 14 hours, as **Fig. B-3** demonstrates.

We derive our support of the preceding observations by investigating the equation proposed by Ramey (1962) for steady-state heat transfer, which is given by

$$\frac{dT}{dz} = -\left(T_{ei} - T_f\right)L_R. \quad \ldots\ldots\ldots\ldots\ldots\ldots (B\text{-}1)$$

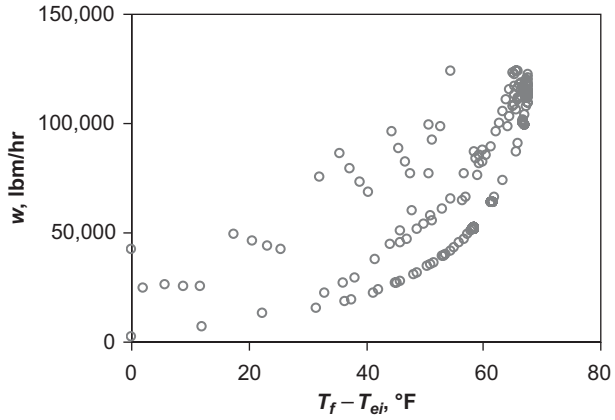

Fig. B-1—Inappropriate U_{to} value of 1.0 produces data scatter.

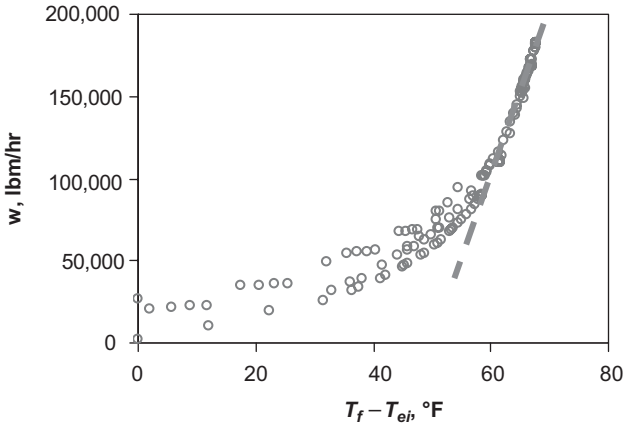

Fig. B-2—U_{to} value of 1.85 produces the expected trend at late times.

By using the definition of relaxation-distance parameter, L_R, given in Eq. A-2, we can rewrite Eq. A-1 as

$$\frac{dT}{dz} = -\left(T_{ei} - T_f\right)\frac{2\pi}{wc_p}\left[\frac{r_{to}U_{to}k_e}{k_e + r_{to}U_{to}T_D}\right]. \quad \text{(B-2)}$$

Manipulating,

$$w\frac{dT}{dz}\frac{k_e + r_{to}U_{to}T_D}{r_{to}U_{to}k_e}\frac{c_p}{2\pi} = \left(T_f - T_{ei}\right). \quad \text{(B-3)}$$

All the parameters on the left-hand side, excluding mass-flow rate, can be lumped together as

$$C = \frac{dT}{dz}\frac{k_e + r_{to}U_{to}T_D}{r_{to}U_{to}k_e}\frac{c_p}{2\pi}. \quad \text{(B-4)}$$

Because the methodology for temperature-difference/mass-flow-rate relationship is applied to a single point in the wellbore, the derivative of temperature value with respect to depth remains constant in the volume considered. All the other parameters become weak functions of time after steady-state heat flow is reached. With appropriate assumptions, Eqs. B-3 and B-4 may be combined to yield a simple relationship between the mass-flow rate and temperature difference, which is given by

$$wC = \left(T_f - T_{ei}\right). \quad \text{(B-5)}$$

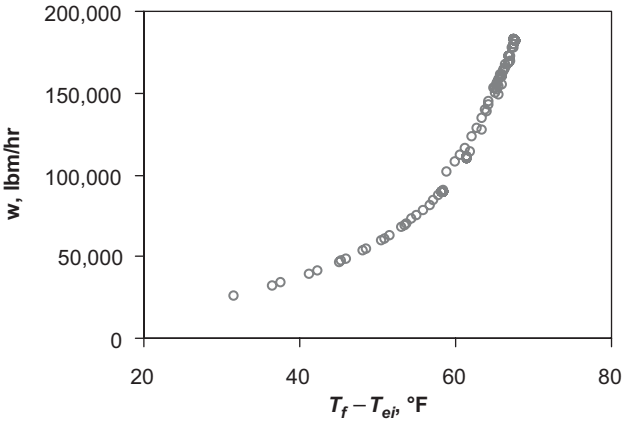

Fig. B-3—Less-ambiguous rate/temperature-difference relationship emerges after 14 hours.

Bulent Izgec is a petroleum engineer at Chevron Energy Technology Company in Houston. email: bizg@chevron.com. His work experience and research areas cover reservoir/production engineering, integrated production modeling, geomechanics, and reservoir simulation. Izgec holds a BS degree in geophysical engineering from Ankara University, Turkey, and MS and PhD degrees in petroleum engineering from Texas A&M University. **Rashid Hasan** is a professor of chemical engineering at University of Minnesota-Duluth. He has 30 years of teaching and research experience in many areas, including fluid and heat flows in wellbores and pressure-transient testing. He has consulted with and offered short courses for oil operating and service companies. He has also worked with NASA on various aspects of multiphase flow and thermohydraulic transients. Hasan has been published extensively and has served on various SPE committees, including editorial review for *SPEPF* and *SPEJ*. He holds MS and PhD degrees from University of Waterloo, Canada. **Dongqing (Don) Lin** is a research specialist in the Agricultural and Biosystems Engineering Department at the North Dakota State University in Fargo. His research interests include mathematical modeling and computer simulation, multiphase flow, and heat transfer. He has experience in conceptual temperature modeling and programming for various systems. Lin worked as an engineer for the China Petroleum & Chemical Corporation (SINOPEC) in Beijing and Malaysia. He was also a senior software developer at the Hematology Algorithm group of Beckman Coulter Inc. in Miami. Lin holds MS and PhD degrees from the University of North Dakota and a BS degree from the Tsinghua University, China. **Shah Kabir** is a senior reservoir engineering advisor at Hess in Houston. email: skabir@hess.com. His experiences include transient testing, wellbore fluid- and heat-flow modeling, and reservoir engineering. Kabir has published two books and approximately 100 papers. He coauthored the 2002 SPE book titled *Fluid Flow and Heat Transfer in Wellbores*. He also contributed in the 2009 SPE monograph on *Transient Well Testing*. Kabir holds an MS degree in chemical engineering from the University of Calgary, Canada. He has served on various SPE committees, including editorial review committees for *SPEPF, SPEREE,* and *SPEJ*. He received commendation as an outstanding technical editor five times for two different journals, and also received the SPE Western Region's Service Award in 2002. He served as SPE Distinguished Lecturer in 2006–07 and became a Distinguished Member in 2007.